The impact of aerosol optical depth assimilation on aerosol forecasts and radiative effects during a wild fire event over the United States

Dan Chen[1], Zhiquan Liu[1]*, Craig S. Schwartz[1], Hui-Chuan Lin[1], Jeffrey D. Cetola[2], Yu Gu[3] and Lulin Xue[1]

1. National Center for Atmospheric Research, Boulder, Colorado, USA
2. Air Force Weather Agency, Omaha, Nebraska, USA
3. University of California, Los Angeles, Los Angeles, California, USA

Submitted to Geoscientific Model Development

Revised in September 2014

*Corresponding author: Dr. Zhiquan Liu (liuz@ucar.edu)

Abstract

The Gridpoint Statistical Interpolation three-dimensional variational data assimilation (DA) system coupled with the Weather Research and Forecasting/Chemistry (WRF/Chem) model was utilized to improve aerosol forecasts and study aerosol direct and semi-direct radiative feedbacks during a U.S. wild fire event. Assimilation of MODIS total 550 nm aerosol optical depth (AOD) retrievals clearly improved WRF/Chem forecasts of surface $PM_{2.5}$ and organic carbon (OC) compared to the corresponding forecasts without aerosol data assimilation. The scattering aerosols in the fire downwind region typically cooled layers both above and below the aerosol layer and suppressed convection and clouds, which led to an average 2% precipitation decease during the fire week. This study demonstrated that even with no input of fire emissions, AOD DA improved the aerosol forecasts and allowed a more realistic model simulation of aerosol radiative effects.

1. Introduction

Aerosols are known to affect weather and climate by modulating radiation in the atmosphere by either scattering or absorption of sunlight (direct effect, e.g. *Rosenfeld et al.,* 2008); thermodynamic effect on clouds (semi-direct, e.g. *Hansen et al.,* 1997); and altering cloud microphysical processes (indirect effects, e.g. *Kaufman and Koren*, 2006). Aerosols can scatter incoming solar radiation and cool both the surface and atmosphere (*Charlson et al.,* 1992; Kiehl and *Briegleb,* 1993). Conversely, absorbing aerosols, such as black carbon (BC) and dust can absorb solar radiation, which heats the local atmosphere (*Hansen et al.,* 1997).

One of the most important short-term effects of aerosols is the impact on local meteorological conditions, especially clouds and precipitation. These changes can be particularly pronounced during biomass burning events when large amount of aerosols are injected into the atmosphere (e.g. *Koren et al, 2004*; *Wilcox et al.,* 2012). Several observational studies have shown evidence for aerosol-induced intensification and weakening of convection with a critical aerosol optical depth (AOD) value (~0.2-0.4), below which additional aerosol enhances convection and precipitation but above which additional aerosol weakens convection and precipitation (*Koren et al.,* 2008; *Rosenfeld et al.,* 2008). For example, *Koren et al.* (2004) analyzed Moderate Resolution Imaging Spectroradiometer (MODIS) satellite data over the Amazon region during the biomass burning season and found that smoke reduced cumulus cloud cover from 38% in clean conditions (AOD of ~0.1) to 0% in heavy smoke (AOD of ~1.3). *Andreae et al*. (2004) used in situ measurements of cloud condensation nuclei and cloud droplets over the Amazon and found that the suppression of low-level rainout by biomass burning smoke tended to invigorate deep convective clouds, thus increasing precipitation. In addition, aerosol-induced changes in the atmosphere may exert different effects on clouds depending on the type

of aerosols (absorbing or scattering) and the vertical distributions of aerosols and clouds (e.g. *Rosenfeld et al.,* 2008).

To accurately simulate aerosol effects, it is necessary to precisely simulate aerosol types and distributions. AOD Data assimilation (DA), combining satellite derived AOD observations with numerical model output, has proved to be skillful at improving aerosol and AOD forecasts (e.g., *Collins et al.,* 2001; *Liu et al.,* 2011). *Liu et al.* (2011, hereafter L11) implemented AOD DA within the National Centers for Environmental Prediction (NCEP) Gridpoint Statistical Interpolation (GSI) three-dimensional variational (3DVAR) DA system coupled to the Goddard Chemistry Aerosol Radiation and Transport (GOCART) (*Chin et al.,* 2000 and 2002) aerosol scheme within the Weather Research and Forecasting/Chemistry (WRF/Chem) model (*Grell et al.,* 2005). Verification results demonstrated improved aerosol forecasts from AOD DA over a week-long period while studying a dust storm in East Asia. This aerosol DA system was also used to assimilate surface $PM_{2.5}$ over the U. S. (*Schwartz et al.,* 2012, hereafter S12) and PM_{10} over China (*Jiang et al.,* 2013).

These previous air-quality oriented studies (L11; S12; *Jiang et al.,* 2013) illustrated the ability of aerosol DA to improve forecasts of total aerosol mass in terms of AOD, $PM_{2.5}$ and PM_{10}, but did not verify aerosol speciation forecasts. As pointed out in L11, the aerosol data assimilation system used here directly analyzes 3D mass concentration of individual aerosol species and allows them to adjust independently with additional constraint from the background error covariance for individual species. Similar method was also adopted by Kahnert (2009) for aerosol inverse modeling. This work builds upon L11 and S12 and serves two purposes. First, this study aims to verify the GSI 3DVAR DA system's capability to analyze and forecast aerosol species, including black carbon (BC) and organic carbon (OC), during a fire event without fire

84 emission input in the WRF/Chem model. Second, the biomass burning aerosol radiative effects
85 (direct and semi-direct) on clouds and precipitation in the downwind region during the fire event
86 are investigated.

87 **2. Model Description and Experimental Design**

88 Version 3.4.1 of WRF/Chem was used and configurations mostly followed S12. The model
89 domain (operationally used at the US Air Force Weather Agency) with 20-km horizontal grid
90 spacing covered a large portion (20-degree north) of the Northern Hemisphere with the polar
91 projection (not shown), although our analysis will focus on North American regions where a
92 wild fire occurred (Fig. 1). There were 57 vertical levels extending from the surface to 10 hPa.
93 Aerosol direct and semi-direct effects were implemented (*Fast et al.*, 2006) in WRF/Chem by
94 linking the optical properties of simulated GOCART aerosols (OC, BC, sulfate, dust and sea salt)
95 to the Goddard Space Flight Center Shortwave radiation scheme (*Chou and Suarez,* 1994).
96 Aerosol optical properties, including scattering/absorption coefficients and single-scattering
97 albedos, are calculated by the "aerosol chemical to aerosol optical properties" module built in
98 WRF/Chem (*Fast et al., 2006*; *Barnard et al.,* 2010). Aerosol indirect effects were not
99 implemented for GOCART with the WRF/Chem version used. The WRF single-moment 6-class
100 microphysics scheme and the Grell-Devenyi ensemble cumulus scheme (*Grell and Devenyi,*
101 2002) were used. Anthropogenic emissions were provided by the 0.5×0.5 degree Reanalysis of
102 the TROpospheric (RETRO) chemical composition over the past 40 years
103 (http://retro.enes.org/data_emissions.shtml) and the 0.1×0.1 degree Emission Database for
104 Global Atmospheric Research (EDGAR) (http://themasites.pbl.nl/tridion/en/themasites/edgar/).
105 Over the U.S., the high resolution (4-km) National Emission Inventory 2005 (NEI'05) emission
106 was used for more accuracy (*Kim et al.,* 2011). Within WRF/Chem, Emissions of dust and sea-

107 salt were parameterized using the GOCART dust and sea-salt modules (*Chin et al.,* 2002). The
108 lateral boundary conditions (LBCs) for meteorological fields were provided by the NCEP Global
109 Forecast System (GFS). LBCs for chemistry/aerosol fields were idealized profiles embedded
110 within the WRF/Chem model as in S12.

111 To evaluate the GSI-WRF/Chem system's capability of improving aerosol species and
112 simulating aerosol radiative effects during the fire event, which originated in the western U.S.
113 and sent smoke eastward during Aug. 13-18, 2012
114 (http://earthobservatory.nasa.gov/IOTD/view.php?id=78881&src=ve), two DA experiments
115 were conducted. One experiment assimilated only NCEP conventional meteorological
116 observations (MET) while the other assimilated both meteorological data and MODIS level-2
117 (10km×10km resolution) 550 nm AOD retrievals obtained from
118 ftp://ladsweb.nascom.nasa.gov/allData/51/MOD06_L2 (and MYD06_L2) (MET_AOD). Only
119 the AOD data flagged as the best quality were used in this study. Each experiment started
120 WRF/Chem simulation with a 6-h cycling interval from 00 UTC 1 August in order to spin up
121 aerosol fields before the fire event. For MET, GSI 3DVAR meteorological (surface pressure, 3D
122 wind, temperature and moisture) analyses (*Wu et al.,* 2012) were performed using the previous
123 cycle's 6 h forecast (meteorological fields only) as the background, and aerosol fields were
124 simply carried over from cycle to cycle (similar to a continuous aerosol forecast). For
125 MET_AOD, GSI 3DVAR updated both meteorological and GOCART aerosol variables (only at
126 18 UTC when AOD data were available over US) every 6 h, again using the previous cycle's 6 h
127 forecast as the background. The assimilation time window was ±1.5-h centered at analysis times
128 (00, 06, 12, and 18 UTC). This cyclic experimental design was also adopted by L11 and S12,
129 who assimilated aerosol observations only. No cross-correlation between meteorological and

aerosol fields was allowed in MET_AOD even though meteorological and AOD data were assimilated simultaneously. More details related to AOD DA can be found in L11 and S12.

This design permitted a clear isolation of the impact of AOD DA. To investigate aerosol radiative effects, 48 h forecasts were initialized at 00 UTC for each experiment during the fire week. Hourly model outputs were analyzed. Since the meteorological fields after 3DVAR DA in the two experiments were very close, the forecast differences of meteorological fields suggest primarily radiative effects due to fire emitted aerosols.

3. PM Speciation Verification

Surface observations, including hourly $PM_{2.5}$ from the EPA AIRNow network and 24h-averaged BC and OC (available every three days) from the Interagency Monitoring of PROtected Visual Environments (IMPROVE) network, were used for aerosol verification. Figure 1 shows the locations of these sites. The averaged AOD differences between the two experiments (MET_AOD minus MET) for the fire period (Aug 14-17) are also shown in Fig 1. Significant increases in AOD (~0.4) over the western U.S. and the fire downwind region (FDR, indicated by the red rectangle in Fig. 1) were produced after assimilating MODIS AOD.

Figure 2 shows the average $PM_{2.5}$, BC and OC observations and model forecasts between August 1-22, 2012 over the sites located in the fire originating area (western U.S. 130-105°W) and fire downwind regions (eastern U.S. 105-70°W). Model outputs from the two experiments were interpolated to the observation sites. The 6-h WRF/Chem forecasts of $PM_{2.5}$ were compared with AIRNow observations at 00, 06, 12, 18 UTC. To compare the forecasts with IMPROVE 24h-averaged (from 06 to 06 UTC) BC and OC observations, the corresponding 6-h model forecasts were also averaged. Observations (black lines) show large peaks in total $PM_{2.5}$, BC and OC during the fire event (Aug. 13-16) in the western U.S., due to strong fire emissions. While

153 the experiment without AOD DA (blue lines) failed to reproduce those peaks and underpredicted
154 aerosol concentrations, most likely a result of the lack of fire emission input in the model, the
155 experiment with AOD DA (red lines) substantially improved surface $PM_{2.5}$ forecasts.
156 Furthermore, the peaks of individual aerosol species' concentrations (especially OC) were well
157 captured with AOD DA, although OC and BC were still underpredicted when the maximum
158 concentrations were reached on 13 August in the Western U.S.

159 Observations also show increased total $PM_{2.5}$ and OC in the downwind region when the smoke
160 was transported eastward during the fire event. MET_AOD improved substantially the
161 simulation with increased OC and $PM_{2.5}$ when compared with MET. While MET exhibits a
162 relatively small bias for BC, large low biases can be seen for $PM_{2.5}$ and OC in both regions even
163 during periods without fire, which may indicate model deficiencies related to emissions and
164 other physical/chemical processes. AOD DA helped correct these biases and improved the
165 simulation for the total mass (i.e., $PM_{2.5}$) and for OC (and to a lesser extent for BC in the
166 Western U.S.) in this case.

167 **4. Aerosol Radiative Feedback**

168 Fire emitted aerosols scatter and absorb solar radiation in daytime and thus can affect the
169 atmospheric temperature profiles. Averaged over the FDR region, which was cloudier than the
170 Western U.S. during the fire period and thus cloud/precipitation features were more likely to be
171 modified through aerosol semi-direct effects, the time series of hourly model outputs of day-2
172 forecasts (i.e., 24h-47h forecasts valid from 00 to 23 UTC) of 550-nm AOD and shortwave
173 downward fluxes reaching the surface (SWDOWN) from the two experiments are shown in Fig
174 3a-b. The jumps in AOD values from 23 UTC to 00 UTC are most likely the result of forecast
175 range differences (i.e., 47h vs. 24h forecast). The average AOD differences reach as high as

176 0.16-0.20 on Aug. 17, which is almost 80% of the total AOD from the MET_AOD experiment.
177 The average AOD differences were around 0.08 after Aug. 20 when fire emissions decreased.
178 The AOD increase led to more aerosol scattering and absorption in MET_AOD, which resulted
179 in a SWDOWN reduction of ~10 w/m^2 during Aug. 15-18 with much smaller changes afterward.
180 Also note that small SWDOWN differences occurred in the late afternoon of Aug. 15, which was
181 likely caused by cloud feedback.

182 Similar to Fig. 3, Fig. 4 shows the FDR-averaged differences of 550-nm AOD, temperature,
183 relative humidity, vertical velocity, cloud liquid and cloud ice water as a function of height and
184 time (hourly output of day-2 forecasts) between the two experiments. The largest AOD (also OC
185 and BC, not shown) increase due to AOD DA occurred at around 4-5 km altitude, indicating
186 upward transport of fire emitted aerosols. This peak AOD height in the AOD DA experiment is
187 consistent with the altitude at which OC and BC had maximum background error variances (not
188 shown). The decreased temperature below this level indicates that the additional aerosols cooled
189 the surface layer and planetary boundary layer (PBL, ~2 km in the afternoon). A weak cooling
190 appeared above the aerosol layer and a weak warming was noted around 15 km. Temperature
191 changed little in the aerosol layer, as the absorbing aerosols (BC and dust) were not dominant in
192 the FDR and no obvious differences of those species were evident between the two experiments
193 (not shown). The relative humidity differences roughly followed the temperature differences,
194 with increased RH in the PBL and above the aerosol layer. Cooler and moister air in the PBL
195 (below ~2km) facilitates low cloud formation from MET_AOD simulations (Aug 17-19), which
196 was especially pronounced on Aug. 17 when the AOD increase reached its maximum. Middle
197 level liquid clouds above the PBL and below the aerosol layer decreased, likely associated with
198 deceased relative humidity. The ice clouds near the tropopause also decreased, which may be

related to the suppression of upward motion in the middle and upper troposphere (Fig. 4b). The aerosol direct and semi-direct effects are consistent with *Jacobson* (2005) and the findings of middle and high cloud suppression are similar to Amazon fire events (*Koren et al*. 2004; *Wu et al.,* 2012).

Figure 3c shows the average precipitation differences (red line, left Y-axis) between the two experiments in the FDR and the corresponding total amount of precipitation (mm/grid) from model forecasts and Stage IV observations (black lines, right Y-axis). Surface precipitation was suppressed: precipitation decreased by up to 0.03 mm/grid (7.3%) late on 16 August and the average precipitation during the fire week was reduced by 2.0%, perhaps associated with the suppressed middle clouds and ice-clouds (Fig. 4d) (*Rosenfeld et al*., 2008). The radiative impact of aerosols on precipitation reported here is consistent with *Zhao et al.* (2011) and *Wu et al.,* (2012), who focused on Asian dust and Amazon fires, respectively. Overall, WRF/Chem produced reasonably good precipitation forecasts when compared to Stage IV observations even though the total amount was usually overpredicted.

5. Summary

The GSI 3DVAR DA system coupled with the WRF/Chem model successfully simulated surface BC, OC, and $PM_{2.5}$ during a wild fire event without any fire emission input in the model. By assimilating total 550-nm AOD retrievals from MODIS sensors, surface $PM_{2.5}$ and OC in the fire originating regions were substantially improved compared to those when AOD was not assimilated. The increased aerosols in the downwind regions were dominated by OC and other oxidized $PM_{2.5}$ components, which are mainly scattering aerosols.

Direct and semi-direct aerosol radiative effects due to aerosols in the downwind region were investigated. Enhanced scattering aerosol concentrations due to AOD DA cooled layers both

below and above the aerosol layer, leading to changes in the temperature, relative humidity, vertical velocity and clouds. We found that the radiative effect of the increased AOD (varied from ~0.2-~0.4) was to increase cloud amount in the PBL and suppress middle level liquid clouds and high level ice clouds. A 2% average reduction of total precipitation due to aerosol increase was also evident. This study demonstrated the value of aerosol DA for more accurately depicting the aerosol spatial distribution and speciation and thus allowed a more realistic model simulation of aerosol radiative effects during a fire event even with no input of fire emissions.

Grell et al. (2011) showed that the inclusion of fire emissions and a plume rise scheme resulted in strong modifications of cloud and precipitation features in high-resolution (10km/2km nested domains) WRF/Chem simulations with both direct and indirect aerosol feedbacks for a wildfire event over Alaska. However, in our initial trials, the inclusion of GOES WF_ABBA (Geostationary Operational Environmental Satellite – Wildfire Automated Biomass Burning Algorithm) (Prins et al., 1998) fire emissions in the simulation of this fire event over California led to a substantial overestimation of aerosol concentrations when compared to surface $PM_{2.5}$, OC and BC measurements (not shown). The impact of AOD DA together with the inclusion of fire emissions will be further investigated in the future.

Acknowledgements

This work is supported by grants from the U.S. Air Force Weather Agency. NCAR is sponsored by the National Science Foundation.

References

Andreae, M. O., Rosenfeld, D., Artaxo, P., Costa, A. A., Frank, G. P., Longo, K. M., and Silva-Dias, M. A. F.: Smoking rain clouds over the Amazon, Science, 303, 1337-1342, DOI 10.1126/science.1092779, 2004.

Barnard, J. C., Fast, J. D., Paredes-Miranda, G., Arnott, W. P., and Laskin, A.: Technical Note: Evaluation of the WRF-Chem "Aerosol Chemical to Aerosol Optical Properties" Module using data from the MILAGRO campaign, Atmos Chem Phys, 10, 7325-7340, DOI 10.5194/acp-10-7325-2010, 2010.

Charlson, R. J., Schwartz, S. E., Hales, J. M., Cess, R. D., Coakley, J. A., Hansen, J. E., and Hofmann, D. J.: Climate Forcing by Anthropogenic Aerosols, Science, 255, 423-430, DOI 10.1126/science.255.5043.423, 1992.

Chin, M., Savoie, D. L., Huebert, B. J., Bandy, A. R., Thornton, D. C., Bates, T. S., Quinn, P. K., Saltzman, E. S., and De Bruyn, W. J.: Atmospheric sulfur cycle simulated in the global model GOCART: Comparison with field observations and regional budgets, J Geophys Res-Atmos, 105, 24689-24712, Doi 10.1029/2000jd900385, 2000.

Chin, M., Ginoux, P., Kinne, S., Torres, O., Holben, B. N., Duncan, B. N., Martin, R. V., Logan, J. A., Higurashi, A., and Nakajima, T.: Tropospheric aerosol optical thickness from the GOCART model and comparisons with satellite and Sun photometer measurements, J Atmos Sci, 59, 461-483, Doi 10.1175/1520-0469(2002)059<0461:Taotft>2.0.Co;2, 2002.

Chou, M.-D., and M.J. Suarez, An efficient thermal infrared radiation parameterization for use in general circulation models, NASA Tech. Memo., TM 104606, vol. 3, 25 pp., NASA Goddard Space Flight Cent., Greenbelt, Md, 1994.

Collins, W. D., Rasch, P. J., Eaton, B. E., Khattatov, B. V., Lamarque, J. F., and Zender, C. S.: Simulating aerosols using a chemical transport model with assimilation of satellite aerosol retrievals: Methodology for INDOEX, J Geophys Res-Atmos, 106, 7313-7336, Doi 10.1029/2000jd900507, 2001.

Fast, J.D., Gustafson, W.I., Easter, R.C., Zaveri, R.A., Barnard, J.C., Chapman, E.G., Grell, G.A., Peckham, S.E.: Evolution of ozone, particulates, and aerosol direct radiative forcing in the vicinity of Houston using a fully coupled meteorology-chemistry-aerosol model, J. Geophys Res-Atmos, 111, D21305. Doi 10.1029/2005jd006721. 2006.

Grell, G. A., and Devenyi, D.: A generalized approach to parameterizing convection combining ensemble and data assimilation techniques, Geophys Res Lett, 29, Artn 1693, Doi 10.1029/2002gl015311, 2002.

Grell, G. A., Peckham, S. E., Schmitz, R., McKeen, S. A., Frost, G., Skamarock, W. C., and Eder, B.: Fully coupled "online" chemistry within the WRF model, Atmos Environ, 39, 6957-6975, DOI 10.1016/j.atmosenv.2005.04.027, 2005.

Grell, G., Freitas, S. R., Stuefer, M., and Fast, J.: Inclusion of biomass burning in WRF-Chem: impact of wildfires on weather forecasts, Atmos Chem Phys, 11, 5289-5303, DOI 10.5194/acp-11-5289-2011, 2011.

Hansen, J., Sato, M., and Ruedy, R.: Radiative forcing and climate response, J Geophys Res-Atmos, 102, 6831-6864, Doi 10.1029/96jd03436, 1997.

Jacobson, M. Z.: Control of fossil-fuel particulate black carbon and organic matter, possibly the most effective method of slowing global warming (vol 107, pg 4410, 2002), J Geophys Res-Atmos, 110, Artn D14105, Doi 10.1029/2004jd005888, 2005.

Jiang, Z. Q., Liu, Z. Q., Wang, T. J., Schwartz, C. S., Lin, H. C., and Jiang, F.: Probing into the impact of 3DVAR assimilation of surface PM10 observations over China using process analysis, J Geophys Res-Atmos, 118, 6738-6749, Doi 10.1002/Jgrd.50495, 2013.

Kahnert, M.: On the observability of chemical and physical aerosol properties by optical observations: Inverse modeling with variational data assimilation. Tellus 61B, 747-755, 2009

Kaufman, Y. J., and Koren, I.: Smoke and pollution aerosol effect on cloud cover, Science, 313, 655-658, DOI 10.1126/science.1126232, 2006.

Kiehl, J. T., and Briegleb, B. P.: The Relative Roles of Sulfate Aerosols and Greenhouse Gases in Climate Forcing, Science, 260, 311-314, DOI 10.1126/science.260.5106.311, 1993.

Kim, S. W., McKeen, S. A., Frost, G. J., Lee, S. H., Trainer, M., Richter, A., Angevine, W. M., Atlas, E., Bianco, L., Boersma, K. F., Brioude, J., Burrows, J. P., de Gouw, J., Fried, A., Gleason, J., Hilboll, A., Mellqvist, J., Peischl, J., Richter, D., Rivera, C., Ryerson, T., Hekkert, S. T. L., Walega, J., Warneke, C., Weibring, P., and Williams, E.: Evaluations of NOx and highly reactive VOC emission inventories in Texas and their implications for ozone plume simulations during the Texas Air Quality Study 2006, Atmos Chem Phys, 11, 11361-11386, DOI 10.5194/acp-11-11361-2011, 2011.

Koren, I., Kaufman, Y. J., Remer, L. A., and Martins, J. V.: Measurement of the effect of Amazon smoke on inhibition of cloud formation, Science, 303, 1342-1345, DOI 10.1126/science.1089424, 2004.

Koren, I., Martins, J. V., Remer, L. A., and Afargan, H.: Smoke invigoration versus inhibition of clouds over the Amazon, Science, 321, 946-949, DOI 10.1126/science.1159185, 2008.

Liu, Z. Q., Liu, Q. H., Lin, H. C., Schwartz, C. S., Lee, Y. H., and Wang, T. J.: Three-dimensional variational assimilation of MODIS aerosol optical depth: Implementation and application to a dust storm over East Asia, J Geophys Res-Atmos, 116, Artn D23206 Doi 10.1029/2011jd016159, 2011.

Prins, E. M., Feltz, J. M., Menzel, W. P., and Ward, D. E.: An overview of GOES-8 diurnal fire and smoke results for SCAR-B and 1995 fire season in South America, J Geophys Res-Atmos, 103, 31821-31835, Doi 10.1029/98jd01720, 1998.

Rosenfeld, D., Lohmann, U., Raga, G. B., O'Dowd, C. D., Kulmala, M., Fuzzi, S., Reissell, A., and Andreae, M. O.: Flood or drought: How do aerosols affect precipitation?, Science, 321, 1309-1313, DOI 10.1126/science.1160606, 2008.

Schwartz, C. S., Liu, Z. Q., Lin, H. C., and McKeen, S. A.: Simultaneous three-dimensional variational assimilation of surface fine particulate matter and MODIS aerosol optical depth, J Geophys Res-Atmos, 117, Artn D13202
Doi 10.1029/2011jd017383, 2012.

Wilcox, E. M.: Direct and semi-direct radiative forcing of smoke aerosols over clouds, Atmos Chem Phys, 12, 139-149, DOI 10.5194/acp-12-139-2012, 2012.

Wu, W. S., Purser, R. J., and Parrish, D. F.: Three-dimensional variational analysis with spatially inhomogeneous covariances, Mon Weather Rev, 130, 2905-2916, Doi 10.1175/1520-0493(2002)130<2905:Tdvaws>2.0.Co;2, 2002.

Wu, L. T., Su, H., and Jiang, J. H.: Regional simulations of deep convection and biomass burning over South America: 2. Biomass burning aerosol effects on clouds and precipitation, J Geophys Res-Atmos, 116, Artn D17209
Doi 10.1029/2011jd016106, 2011.

Zhao, C., Liu, X., Leung, L. R., and Hagos, S.: Radiative impact of mineral dust on monsoon precipitation variability over West Africa, Atmos Chem Phys, 11, 1879-1893, DOI 10.5194/acp-11-1879-2011, 2011.

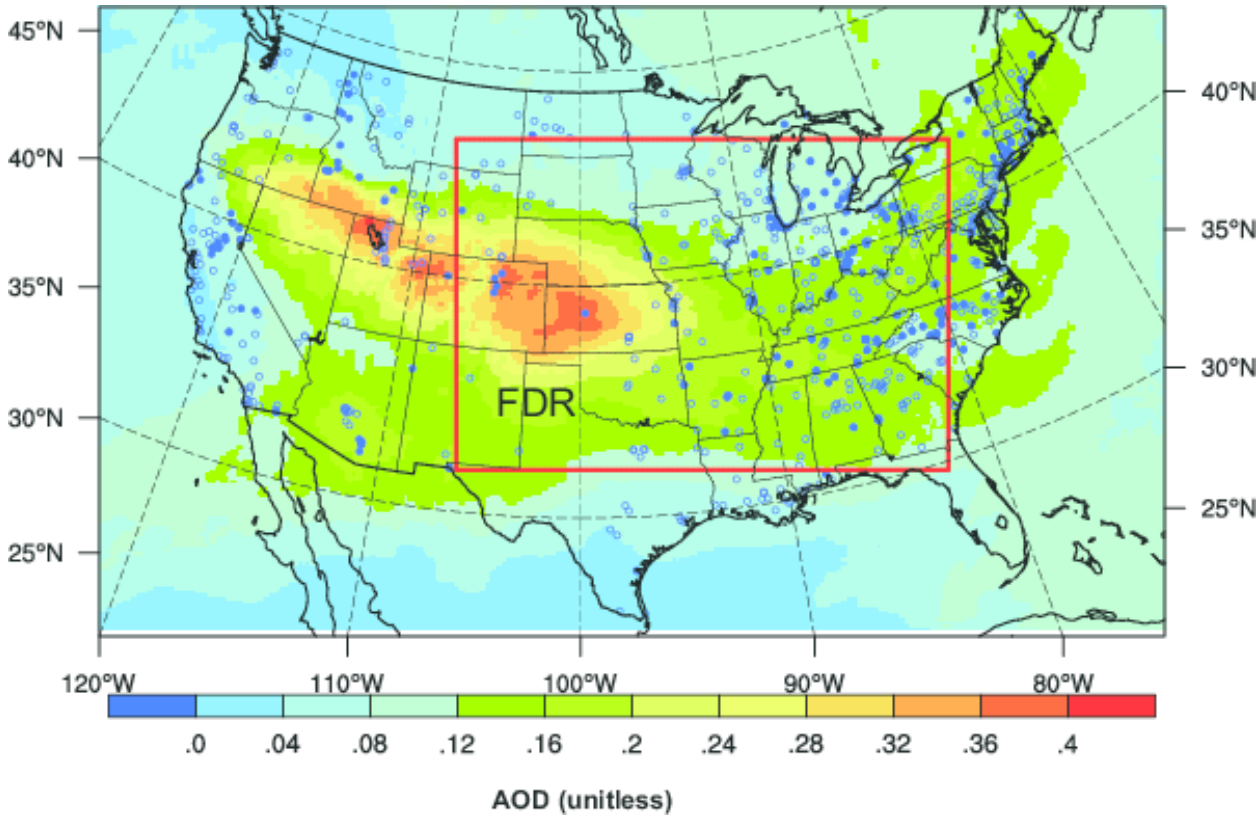

Figure 1. The domain for aerosol verification. The mean AOD difference between the two experiments (MET_AOD minus MET, see text in section 2) for Aug. 14-17, 2012. The locations of AIRNow (open circle) and IMPROVE (dot) sites are also shown. The red rectangle is defined as the fire downwind region (FDR) used in the radiative effect analysis.

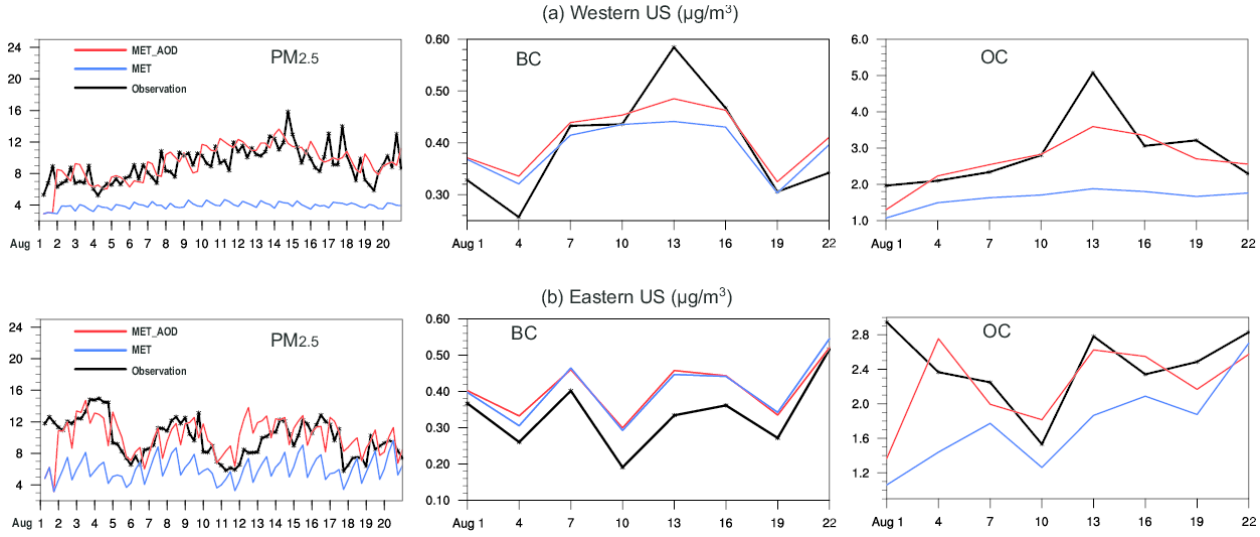

Figure 2. The time series of model predicted (6-h forecasts) and observed $PM_{2.5}$, BC and OC, averaged over the (a) western (130-105°W) and (b) eastern U.S. (105-70°W) during Aug. 2012. $PM_{2.5}$ is in 6-h interval. BC and OC are in 72-h interval.

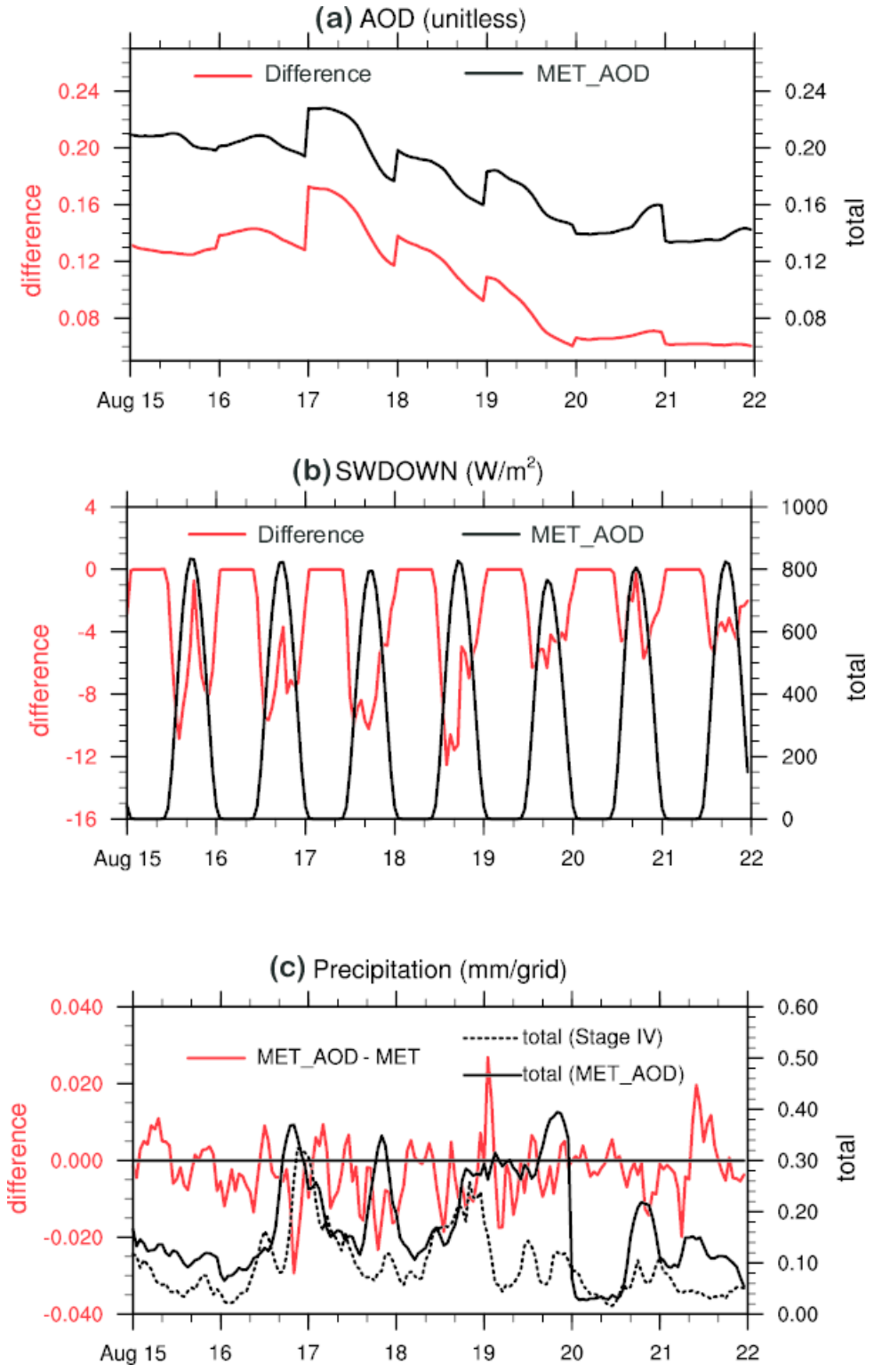

Figure 3. The hourly model output of day-2 forecasts averaged over the FDR for (a) 550-nm AOD, (b) shortwave downward fluxes and (c) precipitation during Aug. 15-21. Red lines: the difference of MET_AOD minus MET (left *Y*-axis); Black lines: the total amount from MET_AOD (right *Y*-axis).

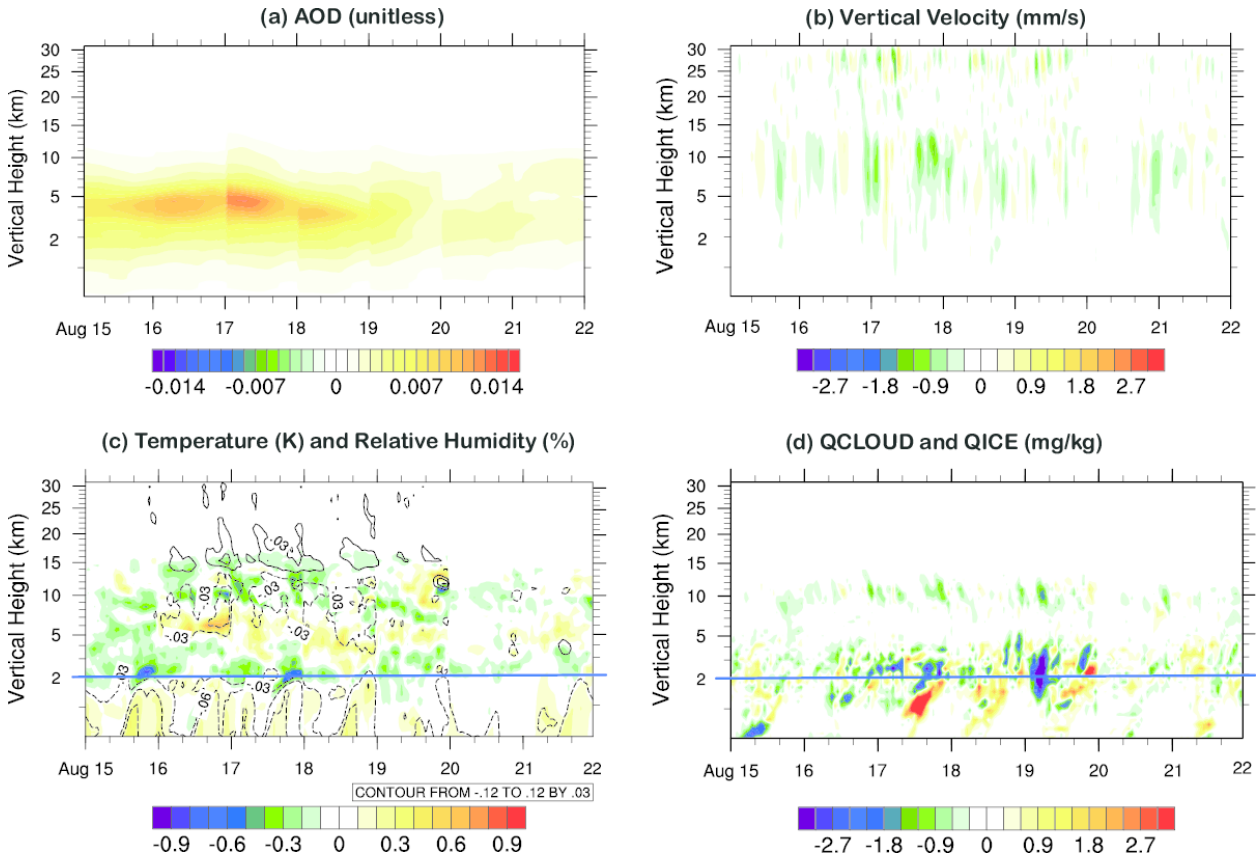

387

388 **Figure 4.** Similar to Fig. 3, but for the FDR averaged differences of MET_AOD minus MET for
389 (a) AOD, (b) vertical velocity, (c) temperature (contours) and relaive humidity (color shaded)
390 and (d) liquid and ice clouds as a function of height and time.

391